Molinero-Fernández, A., López, M.A. and Escarpa, A. (2020) 'Electrochemical Microfluidic Micromotors-Based Immunoassay for C-Reactive Protein Determination in Preterm Neonatal Samples with Sepsis Suspicion', Analytical chemistry (Washington), 92(7), pp. 5048–5054.

Available at https://doi.org/10.1021/acs.analchem.9b05384

(Article begins on next page)

Electrochemical Microfluidic Micromotors-Based Immunoassay for C-Reactive Protein Determination in Preterm Neonatal Samples with Sepsis Suspicion.

Molinero-Fernández, Á. López, M. Á. Escarpa, A.

Abstract

On-line coupling of a micromotor-based immunoassay and a microfluidic electrochemical detection was explored as a new approach for C-reactive protein (CRP) determination in serum and preterm neonatal plasma samples with sepsis suspicion. The approach combines the advantages of micromotors (self-fluid mixing capabilities leading to a faster assay in low sample volumes) and electrochemical microfluidic (flow-controlled ultraminiaturized electrochemical detection, high sensitivity, and low-cost) technologies. Both technologies elegantly meet the *point-of-care-testing* or bed-side device requirements such as low analysis times, miniaturization and simplification, and single use. Anti-CRP functionalized micromotors (anti-CRP-rGO (reduced graphene oxide)/Ni/PtNPs (platinum nanoparticles))-based immunoassay coupled to thin layer Au-based electrochemical microfluidics operating at −0.20 V under controlled fluidic detection operations (30 μL/min) allowed the sensitive (LOD = 0.54 μg/mL) and accurate CRP determination using very low volume preterm neonatal clinical samples (< 10 μL) in just 8 min of total assay time. These excellent analytical characteristics obtained linked to the full automatization of the immunoassay allowed the fast and accurate determination of CRP in hardly available clinical samples as those coming from preterm infants with suspected sepsis. These results demonstrated the usefulness of the approach which meets the clinical requirements as a future point-of-care device for clinical analysis.
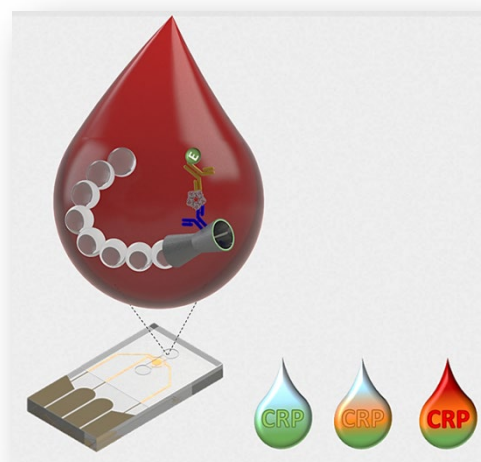
1. Introduction

Micromotors technology has been widely explored in the last few years because it offers new alternatives, especially in clinical diagnostics. Based on their autonomous motion through the transformation of chemical energy or external stimulus (i.e. light, magnetic, ultrasound) into efficient movement, a plethora of relevant applications are currently being developed in several areas,[1] including environmental remediation,[2] drug delivery,[3] and especially in sensing and biosensing of relevant (bio)-molecules as has been recently reviewed.[4] The *on-the-fly* recognition of the analyte by autonomous propulsion of bioreceptor modified motors around a complex sample constitutes a new and exciting paradigm in analytical chemistry.[5,6] Bubble-propelled catalytic micromotors are particularly appropriate for on the fly immunoassays due to their rapid and efficient propulsion in complex media as well as their self-fluid mixing effect, which enhances the kinetics of the recognition event leading to a faster and sensitive assay.[7–10] In this sense, using self-propelled micro-/nanomotors functionalized with selective bioreceptors, especially antibodies, different targets such as tumoral cells,[11] cancer biomarkers,[12] proteins,[13] spores of *Bacillus anthracis*,[14] *Staphylococcus aureus*,[15] or cortisol[16] with optical detection have been recently developed.

Despite the proven potential and novel developments, the possibilities of micromotors in the analytical field remains largely unexploited, mainly due to the infancy of the field and the drawbacks to perform appropriate signal transduction and detection with typical analytical instrumentation. Most of the micromotors' approaches use fluorescence microscopy or electrochemical detection.[17] While fluorescence microscopy is not suitable for *points-of-care$_s$* (POCs), electrochemical detection fits perfectly to these devices thanks to its high sensitivity and inherent miniaturization. In this sense, the development of ultraminiaturized microfluidic detectors, which allows the full three-electrodes integration for flow operations and its combination with micromotors technology, is a very interesting approach for POC development.

Up to now, the electrochemical detection using micromotors has only been used in off-line approaches, where the transduction step is commonly performed in discontinuous mode and it takes place far from the micromotor operation environment. Thus, the off-line detection of micromotors constitutes a major limitation yet, not only in terms of rapid response and simplicity, but also because it avoids the complete monitorization of the process at real time, losing useful chemical information.

Taking in mind the exposed above, the coupling of micromotor-based immunoassay to the electrochemical microfluidic detection systems is highly pertinent, since it adds to the excellent characteristics of micromotors stated above for *on-the-fly* biorecognition event, the possibility to perform an easy automation of the whole process at the same time that allows portability and potential development of POCs devices.

C-reactive protein (CRP) has demonstrated to be a good biomarker of neonatal infections and its prognosis after antibiotic therapy.[18,19] Values higher than 10 µg/mL in blood can be considered positive for sepsis. However, to improve diagnosis and disease monitoring, serial analysis is needed. This aspect constitutes an additional problem, especially for those patients where low volume samples are available such as neonates. Hence, the development of reliable, cost-effective, sensitive, low sample volume and rapid-based approaches for CRP detection and monitoring could help to reduce mortality and avoid potential antibiotic resistances and severe side effects in these patients. Nowadays, CRP determination is carried out by different immunochemical laboratory techniques (ELISA, immunoluminescence and immunoturbidimetric assay).[20] However, and despite of their sensitivity, these methodologies require of central laboratories and results are not fast enough, being highly incompatible with the need to make quick decisions. Looking to solve these limitations, some microfluidic based approaches for electrochemical detection of CRP have been previously developed.[20-22] However, they present complex architectures, required high analysis time and relatively larger volume of sample. Consequently, the new coupling of the electrochemical microfluidic with self-propelled micromotors is a pertinent approach, which could meet the clinical needs.

In this work, a micromotor-based immunoassay coupled to an electrochemical microfluidic chip has been designed for CRP determination. This assay makes use of the extraordinary capability of these antibody-functionalized micromotors to swim through the low sample volumes and specifically recognize the target, combined with those derived from microfluidic electrochemical detection which offers a complete miniaturization without loss of performance and high sensitivity, meeting the POC's requirements.

To the best of our knowledge, this is the first report coupling a micromotor-based immunoassay with electrochemical microfluidic detection involving an application of the high significance as the CRP determination in very low sample volumes from preterm neonates with sepsis suspicion.

2. Materials and methods

2.1. Reagent and solutions

CRP (8C72) and two paired monoclonal mouse antihuman CRP antibodies (4C28C HRP-conjugated and 4C28B biotinylated) were obtained from HyTest (Turku, Finland).

Dilution of CRP and antihuman CRP antibodies were prepared in PBS, 0.1 M phosphate (Scharlau, 99%), 0.138 M NaCl (Scharlau, 99%), and 2.7 mM KCl (Scharlau, 99%), buffer solution pH 7.5.

Enzyme substrate PERDROGEN 30% H_2O_2, hydroquinone, bovine serum albumin (BSA), Streptavidin, 1-ethyl-3-(3- (dimethylamino)propyl) carbodiimide (EDC), and N-hydroxysuccinimide (NHS) were purchased from Sigma-Aldrich (Madrid, Spain). Hydroquinone and peroxide solutions were prepared in phosphate buffer 0.1 M, pH 7 (PB). EDC, NHS, and streptavidin solutions were prepared in MES buffer 0.1 M pH 5. MES monohydrate was obtained from Sigma-Aldrich.

Commercial food dyes were obtained from Hacendado retail market (Spain).

Five μm-diameter conical pore polycarbonate membranes (PC) (Catalog No. 7060-2513) were purchase from Whatman (Maidstone, UK). Graphene oxide (GO, 2 mg/mL dispersion in water, Catalog. No. 763705) and Chloroplatinic acid

hydrate (Catalog No.254029) were obtained from Sigma- Aldrich (Madrid, Spain) and used without further purification.

2.2. Samples

European Reference Material ERM-DA474/ IFCC, with a CRP concentration of 41.2 ± 2.5 µg/mL, was obtained from Sigma-Aldrich (Madrid, Spain).

Hospital Clínico San Carlos (Madrid, Spain) provided unique plasma samples from preterm neonates with sepsis suspicion. The study was approved by the Ethics Committee of the Hospital and parental informed consent was obtained before the collections of blood samples. Babies were included in the study since their blood samples were needed as part of the standard care in the intensive care unit and not for the only purpose of the present study.

2.3. Apparatus

Amperometric measurements were carried out with a multi potentiostat/galvanostat, µSTAT 8000 from Metrohm DropSens, (Oviedo, Spain), which incorporates the software "DropView 8400". Inverted optical microscope (Nikon Eclipse Instrument Inc. Ti-S/L100), Zyla sCMOS camera and NIS element software were used for capturing images and tracking the speed of micromotros. An epifluorescence attachment with a G-2A filter cube were used for fluorescence measurements. Scanning electronic microscopy (SEM) images were obtained with a JEOL JSM 6335F instrument at an acceleration voltage of 22 kV. EDX mapping was performed with an EDX detector attached to the SEM instrument.

2.4. Electrochemical microfluidic setup

Electrochemical flow cell all-in-one (AIO), "wall-jet" flow cell add-on for standard thin-film electrodes (AIO-ADD-ON-FC) and gold thin-layer microfluidic single-electrode (SE) TL-SE1-Au were obtained from Micrux technologies, (Oviedo, Spain) (**Figure V.3.1A**). The SE used (10 × 6 × 0.75 mm) integrates the three Au electrodes: working electrode (0.3 mm^2) (WE), auxiliary electrode (AE) and counter electrode (CE). Microchannel width is 250 µm/1 mm (EC cell) and 40 µm height (**Figure V.3.1B**). Harvard Pump 33 Dual Syringe Pump from Harvard Apparatus and syringe Omnifix-F 1 mL from BRAUN were used for generating the hydrodynamic flow. Needle Sterican 25Gx1 1/2″ - 0,8 × 40 mm

from BRAUN was used as external reservoir. A scheme of the complete setup is showed in **Figure V.3.1C**.
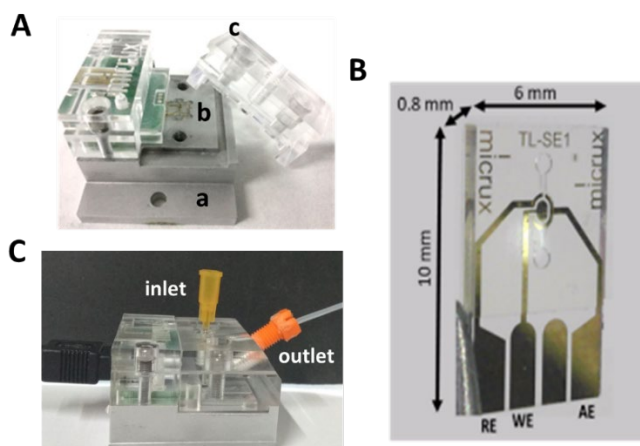
Figure V.3.1. Electrochemical microfluidic setup. (A) Electrochemical flow cell platform (a) with the thin-layer microfluidic single-electrode (b) and "wall-jet" flow cell add-on (c). (B) Gold thin-layer microfluidic single-electrode. (C) Electrochemical microfluidic setup with external reservoir (inlet) and thread connection (outlet).

2.5. Micromotors synthesis.

The electrochemically reduced graphene oxide (rGO) micromotors were prepared by electrochemical reduction of graphene oxide into 5 µm-diameter conical pores of a polycarbonate membrane (PC) following an optimized protocol.[23,24] The S4 branched side of the membrane was treated with a sputtered thin gold film to perform as a working electrode. The membrane was assembled in a Teflon plating cell with aluminum foil serving as an electrical contact to the working electrode for the subsequent electrodeposition. Graphene oxide (GO, 0.5 mg/mL) was first dispersed in a solution containing 0.1 M H_2SO_4 and 0.5 M Na2SO4 in an ultrasonic bath for 15 min. The simultaneous electrochemical reduction and deposition of GO was carried out using cyclic voltammetry (CV, over +0.3 to −1.5 V vs Ag/AgCl (3 M KCl), at 50 mV s^{-1}, for five cycles; n = 5), using a Pt wire as counter electrode. Also, a magnetic layer of Ni was incorporated in the micromotor structure for efficient magnetic control of the micromotor. The nickel tube layer was plated inside the reduced carbon layer by the galvanostatic method. First, 10 pulses of −20 mA were applied for 0.1s to generate nucleation spots. Then, a constant current of −6 mA was applied for 300 s to grow the nickel layer. The inner platinum nanoparticles layer (PtNPs) was

deposited by amperometry at −0.40 V for 750 s from an aqueous solution containing 4 mM of H_2PtCl_6 in 0.5 M acid boric. The sputtered gold layer was gently hand polished with 1 μm alumina slurry. After that, the membrane was dissolved in methylene chloride for 30 min to completely release the microtubes. The microrockets were placed on the magnet holding block, and the supernatant was removed. Afterward, successive washes with isopropanol and ethanol (both twice) and ultrapure water (18.2 MΩ.cm, three times) were performed respectively, with a 2 min on the magnet holding block between each wash. All microtubes were stored in ultrapure water at room temperature when not in use. The template preparation method resulted in a reproducible micromotors synthesis.

2.6. Micromotors functionalization

1-Ethyl-3-(3-(dimethylamino)propyl) carbodiimide (EDC) / N-hydroxysulfosuccinimide (NHS) chemistry was used to activate the carboxyl-terminated groups from the carbon materials layer for conjugation with streptavidin. For this purpose, a stock solution of 800 μL (160000 microengines approximately) was treated with 200 μL of a 100 mM EDC/NHS solution prepared in 0.1 M MES buffer, pH 5.0, for 30 min at 25 °C. After two washing steps with MES buffer, the activated micromotors were incubated with 200 μL of a 200 μg/mL streptavidin solution in 0.1 M MES buffer, pH 5.0, for 1 h at 25°C. Two washing steps with MES buffer and an additional washing step with PBS were carried out to eliminate the excess of streptavidin.

Then, streptavidin modified micromotors were incubated in a solution containing 1000 μL of 10 μg/mL biotinylated anti-CRP antibody (capture antibody). After room temperature incubation under stirring for 30 min, the tube was placed on the magnetic holding block and the supernatant was removed. Immediately, it was followed by twice-washing steps with 1000 μL of PBS buffer and the micromotors were resuspended in 800 μL of PBS and maintained at 4 °C.

2.7. Microfluidic micromotor-based immunoassay.

Approximately 1600 of the specific antibodies functionalized micromotors were brought into the external reservoir of the microfluidic platform. Then, only 10 μL

containing the CRP standard or sample solution, the HRP-labeled anti-CRP secondary antibody (10 µg/mL), and the micromotors fuel (1% H_2O_2 + 1.5% surfactant) were added together to the reservoir allowing their active swimming for 5 min. In the course of this time, self-propelled micromotors capture the target analyte and the secondary labeled antibody on-the-fly performing the sandwich immunocomplexes in a single step. Then, micromotors movement was stopped by the addition of PBS. The suspension was flowed into the microfluidic platform by aspiration thanks to a syringe pump. Magnetic micromotors modified with the built immunocomplexes, and thanks to their intermedium nickel layer, were just retained into the metallic channel of the external reservoir by the aid of a magnet, while the reaction solution is washed away with the PBS stream. An additional washing step was performed by flowing PBS at 50 µL/min for 2 min.

A solution containing the enzymatic substrates HQ (0.9 mM) and H_2O_2 (5 mM) (final concentrations) was continuously flowed over the integrated Au-working electrode at 30 µL/min, while the amperometric measurement was accomplished after 60 s, at −0.20 V detection potential.

3. Results and discussion

A scheme of the electrochemical microfluidic micromotor-based immunoassay (EMMIm) is represented in **Figure V.3.2**.
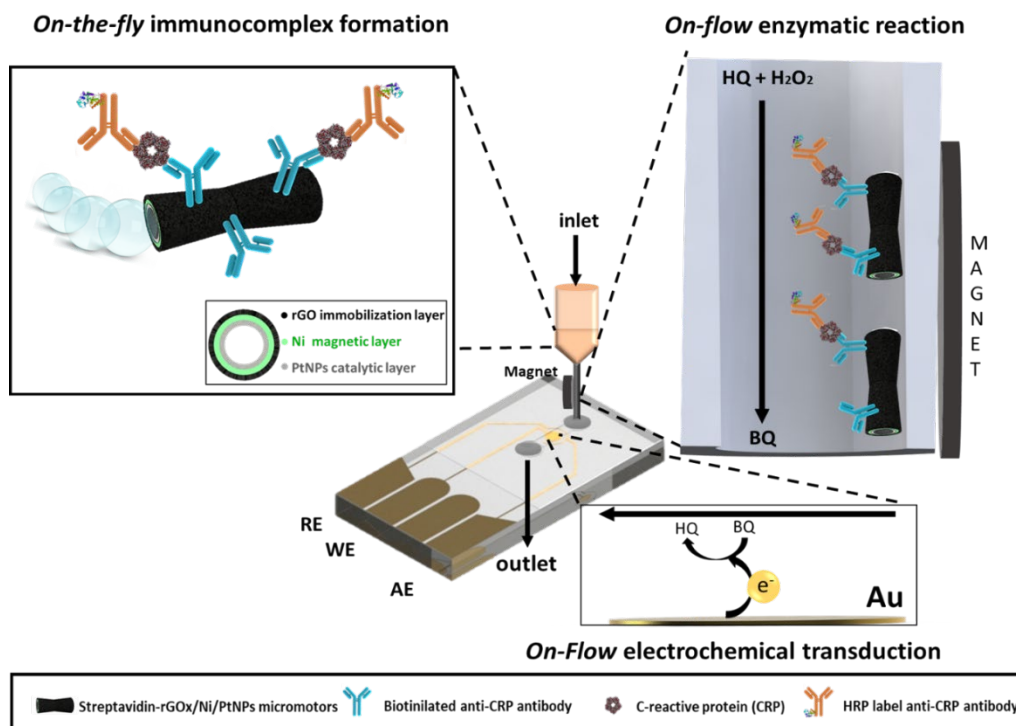
Figure V.3.2. Magnetic micromotor-based immunoassay on board of an electrochemical microfluidic chip for CRP determination.

The strategy combines the advantages of using anti-CRP functionalized micromotors capable of swimming autonomously around the sample to bind actively the specific analyte, with the benefits of the electrochemical detection within a microfluidic chip for CRP determination in sepsis diagnosis. Specifically, tailored anti-CRP-rGO/Ni/PtNPs micromotors combine the rGO functionalization capabilities (rGO, outer layer), together with magnetic (Ni, intermediate layer) and catalytic (PtNPs, inner layer) properties for micromotor guidance and controlled bubble propulsion, respectively.

Our hypothesis is that the efficient propulsion of anti-CRP-rGO/Ni/PtNPs micromotors and the generated microbubbles tails, favoring the fluid mixing, improves the efficiency of the antibodies-antigen interactions. The *on-the-fly* construction of the sandwich immunocomplex was performed within an external reservoir in line with the electrochemical microfluidic platform. To carry out the electrochemical detection within the microchip, anti-CRP micromotors were flowed inside and magnetically retained in the metallic channel of the external reservoir. Hence, the enzymatic substrates were continuously flowed through,

and the electrochemical product related to the CRP concentration that was amperometrically measured.

Figure V.3.3A illustrates the steps involved in the electrosynthesis and functionalization of the catalytic tubular anti CRP-rGO/Ni/PtNPs micromotors. **Figure V.3.3B** shows the SEM and EDX images of the electrosynthesized rGO/Ni/PtNPs micromotors. The SEM images illustrate their tubular shape (controlled by the membrane porous size (5 μm) with a 5 μm width, 10 μm length) while EDX ones confirm the composition of the tailored layers.

The presence of the streptavidin molecules, covalently bounded through the EDC/NHS chemistry onto the surface of rGO outer layer micromotors, was studied by the utilization of a biotin-fluorophore labeled reagent (Atto 550-biotin). In this sense, streptavidin-modified micromotors after a blocking step (5% (w/v) BSA) were incubated in a solution of biotin-fluorophore labeled reagent (20 μg/mL) during 15 min, which after adequate washing steps were fluorometrically detected. **Figure V.3.3C** confirms the presence of fluorescence onto the micromotors surface, which can be attributed to the presence of an elevated amount of streptavidin bound to the outer layer of the micromotors.

The propulsion of the anti-CRP-rGO/Ni/PtNPs was also studied. Time-lapse images (**Figure V.3.3D**), illustrate the efficient propulsion of the rGO/Ni/PtNPs micromotors after the antibody functionalization. As expected, the speed decreased from 170 ± 30 μm s^{-1} to 130 ± 40 μm s^{-1} after functionalization, which can be attribute to the on-board protein immobilization. However, as we will discuss later, this fact did not affect the practical application of micromotors.
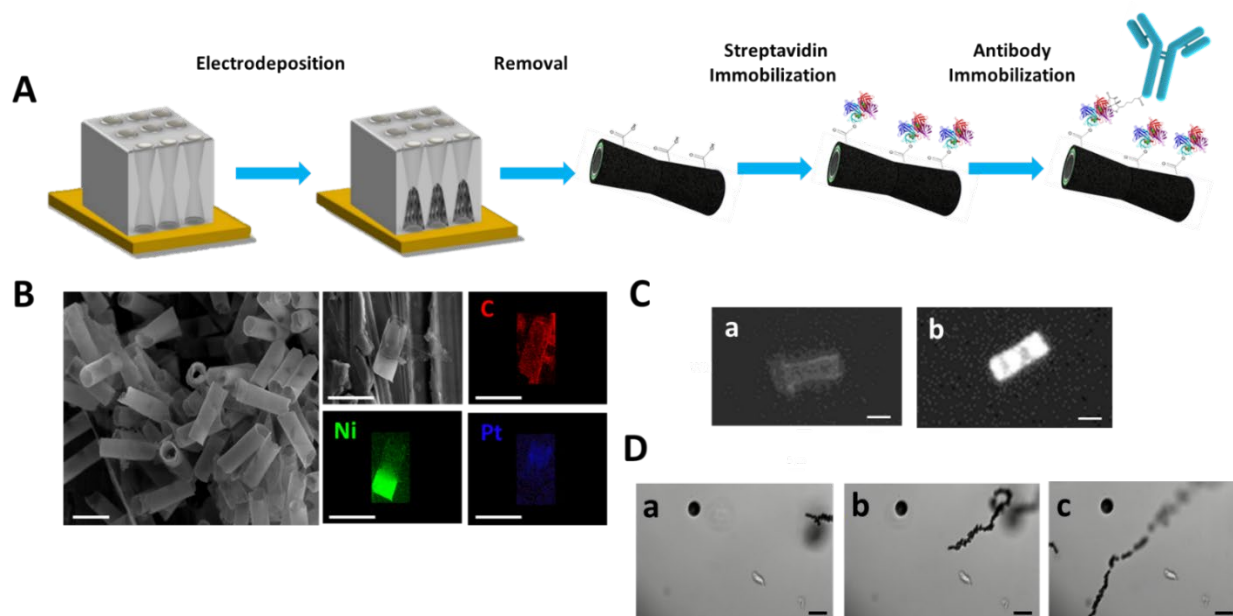
Figure V.3.3. (A) Schematic of the preparation of rGO/Ni/PtNPs micromotors and their functionalization with anti-CRP capture antibody. (B) SEM and EDX analysis of rGO/Ni/PtNPs micromotors. Scale bar: 10 µm. (C) Fluorescence microscopy images of rGO/Ni/PtNPs micromotors: without (a) and with streptavidin after incubation with Atto 550-Biotin (b). Scale bar: 5 µm (D) Time-lapse images of the efficient navigation of functionalized micromotors: 0 s (a), 1.5 s (b), 3 s (c). Conditions: PBS containing 1% H_2O_2 and 1.5% NaCh. Scale bar: 40 µm.

Micromotor-based *on-the-fly* immunoassay was previously optimized. The optimal concentrations for capture and detection antibodies were 10 µg/mL for both. Cathodic current increased with higher antibody concentrations up to the optimal concentration followed by a plateau as indicative of saturation of binding sites. In order to diminish nonspecific adsorption onto the micromotors surface, a blocking step with BSA (2.5% (w/v)) during 30 min after capture antibody immobilization was carried out, reducing the unspecific response to a value lower than 1%. Chemical fuel (H_2O_2 1% (v/v)) and surfactant (NaCh 1.5% (w/v)) as well as number of micromotors (≈ 1600) and *on-the-fly* capture time (5 min) were also optimized to obtain the best immunoassay performance.

Once the anti-CRP micromotor-based biorecognition events take place under the optimized conditions in the external reservoir, the on-line electrochemical detection was optimized into the microfluidic platform. Hence, enzymatic substrate and electrochemical mediator concentrations, flow rate, and detection potential were carefully evaluated. The tested ranges and the selected values for each condition are summarized in **Table V.3.1**. Flow rate (30 µL/min) as well as enzymatic substrate (5 mM) and mediator (0.9 mM) concentrations were

adequately chosen to obtain the highest amperometric signal. Hydrodynamic voltammograms of immunocomplex-micromotor were constructed from 0 to −0.50 V, where the best signal-to-noise characteristics were obtained at −0.20 V, with this value being chosen for the next experiments.

Table V.3.1. Microfluidic electrochemical detection optimization.

Parameter	Tested Range	Selected Value
F, μL/min	10−70	30
[HQ], mM	0−10	0.9
[H_2O_2], mM	1−15	5
E, V	0 to −0.5	−0.2

One of the advantages of our approach is that the immunocomplex formation by the bubble propelled micromotors was carried out in an external on-line coupling reservoir (faraway of the electrode). Then, this solution was hydrodynamically flowed outside the microchip, while the enzymatic substrate solution was carried out through the magnetically retained micromotors toward the microfluidic electrochemical detector. Hence, no effect on electrochemical sensing due to bubbles was observed.

In order to evaluate the effectiveness of the self-propelled micromotors mixing effect, a static control was carried out (**Figure V.3.4**).

As expected, a tremendous decrease of the intensity current (75%) was observed when static micromotors were used (absence of H_2O_2 fuel) in comparison with micromotor approach (**Figure V.3.4A**).The effectiveness of the self-propelled micromotors was also evaluated toward the mixing of two food dyes (blue and yellow) to generate a green one using the previous approaches and compared with the static conditions (**Figure V.3.4B**). As can be observed, only 2 min were needed to obtain a homogeneous dye mixture when micromotors were properly used (b) in contrast with the static conditions, which did not reach the homogeneous dye mixture even after 10 min (a). The enhanced micromotor behavior in these small volumes, can be attributed not only to the active finding of the analyte around the solution by the self-propelled anti-CRP micromotors but also to the inherent self-fluid mixing effect of micromotors.
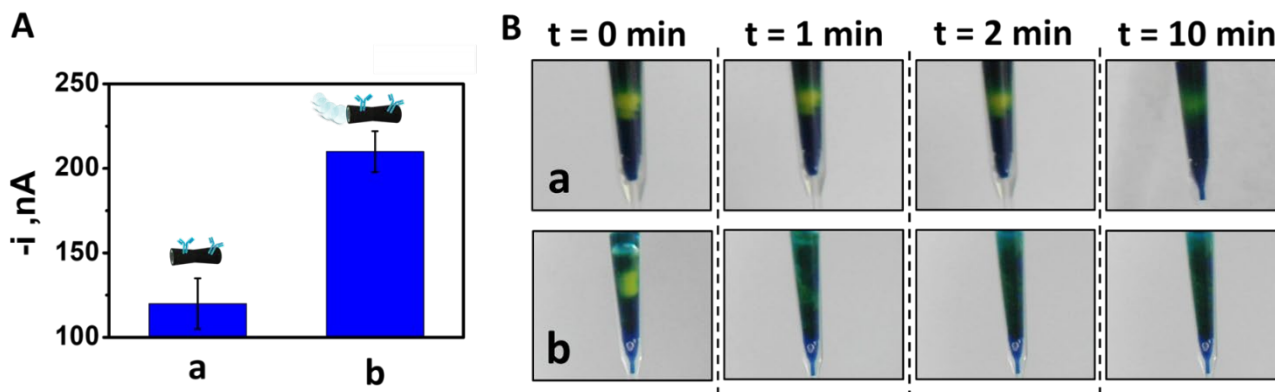
Figure V.3.4. Effectiveness of EMMIm. (A) Amperometric current intensity obtained at static (a) and micromotor-based conditions (b). (B) Effect of induced mixing by micromotors of a dye mixture in an external reservoir using static conditions (without micromotors movement) (a), micromotor-based approach (1% H_2O_2; 1.5% NaCh) (b).

Then, the analytical capabilities of EMMIm to determine CRP at clinically relevant sepsis stages were deeply evaluated. First, **Figure V.3.5** shows the calibration plot and equation for CRP determination using the EMMIm approach. LOD and LOQ of 0.40 µg/mL and 1.0 µg/mL were obtained according to the S/N = 3 and S/N = 10 criteria, respectively (S was estimated as sd (n = 10) obtained during the measurement of the current intensity from the lowest CRP concentration used in the calibration, 1 µg/mL). Linear working range (1−100 µg/mL) allowed CRP determination at the clinically relevant concentrations (sepsis CRP cut-off = 10 µg/mL), revealing the suitability of the EMMIm for determination of CRP biomarker in sepsis diagnosis. Precision was also evaluated at CRP concentration of 10 µg/mL. The intra-assay precision reached an CV value of 7.0% (n = 5) for EMMIm performed in the same day; an inter-assay precision of 10% (n = 5) for EMMIm performed in different days.
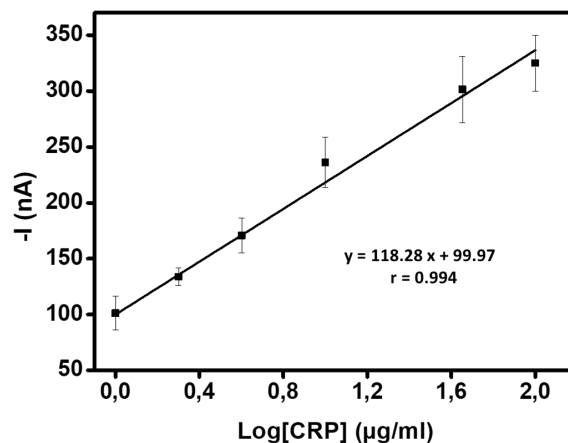
Figure V.3.5. Calibration plot for CRP determination using EMMIm approach (5 min, 1.5% NaCh, 1% H_2O_2, n = 3).

Second, serum certified reference material (CRM) and high significance plasma samples from preterm neonates with sepsis suspicion were analyzed. The results obtained are listed in **Table V.3.2**. The analysis of CRM serum revealed a good accuracy of the micromotor-based method, even at different dilutions. Besides, the results obtained by our EMMIm were highly in agreement with those declared by the Hospital (BRAHMS CRPus KRYPTOR) for preterm neonate plasma samples. It is worthy to remark the ability of the developed EMMIm to analyze serum and plasma samples without any dilution, and within the entire relevant concentrations range, allowing us to distinguish not only between healthy and ill conditions, but different severities of infection and probability of sepsis too (see color code in **Table V.3.2**). Each neonatal sample was analyzed in a different period (when the patient was rolled on into the Neonatal UCI), using the micromotors and antibodies batch available at that time, and hence demonstrating indirectly the good reproducibility in the developed approach. Overall, these results revealed the applicability of our approach for clinically relevant sample analysis.

Finally, propulsion of the anti-CRP-rGO/Ni/PtNPs micromotors was also evaluated in the blood matrices assayed. As can be observed in **Video V.3.S1**, the micromotors speed did not decrease significantly in serum (120 ± 40 µm s^{-1}). However, in plasma samples, the fuel conditions had to be adjusted to obtain an adequate motion (150 ± 30 µm s^{-1}), being needed an increasing of H_2O_2 concentration from 1 (in PBS buffer, or CRM serum) to 2% (in plasma samples

from preterm neonates). However, this fact did not affect the practical application of our micromotors, as has been demonstrated during the analysis of the samples, as was demonstrated above. To confirm this, the influence of H_2O_2 levels (0−5%) on immunoassay performance was also evaluated. To this end, anti-CRP micromotors (electrosynthesized without PtNPs catalytic layer) were left under external stirring conditions (5 min, 950 rpm. 1.5% NaCh) for each fuel level. No differences were observed when H_2O_2 levels below 3% were assayed, confirming that the fuel conditions used (1% for PBS and CRM serum, 2% for plasma samples from preterm neonates) did not influence on the overall EMMIm performance.

Table V.3.2. Analysis of serum reference material and preterm neonate plasma samples.[a]

CRM Serum Sample	[CRP]$_{obtained}$(µg/ml)		[CRP]$_{reference}$(µg/ml)	
Raw material	39 ± 3		41.2 ± 2.5	
1/10 dilution	4.0 ±0.2	40 ± 2	4.1 ±0.3	41.2 ±2.5
1/20 dilution	1.9 ±0.1	37 ± 2	2.1 ±0.1	41.2 ±2.5
Neonatal Plasma Samples	[CRP]$_{obtained}$(µg/ml)		[CRP]$_{reference}$(µg/ml)	
No suggestive of sepsis(n=3) (Patient final diagnosis: Healthy)	2.3 ± 0.3		< 2.9	
Possible suggestive of sepsis(n=3) (Patient final diagnosis: Extreme prematurity)	32 ± 3		34.0	
Highly suggestive of sepsis(n=3) (Patient final diagnosis: Sepsis)	63 ± 5		58.4	

[a] Results are expressed as mean values ± SD (n = 3). Color code: green, orange, and red for CRP levels with low, moderate, and high rate suggestive of sepsis, respectively.

4. Conclusions

Analytical capabilities of smartly functionalized anti-CRP-rGO/Ni/PtNPs micromotors coupled to an electrochemical microfluidic chip, integrating thin-layer Au electrode operating at −0.20 V; offered an automated, accurate and fast

(8 min) CRP determination in preterm infants' plasma samples using less than 10 µL of sample.

This new approach becomes a promising tool for on-site/bed-side clinical analysis, especially in those fields where limited sample amount is available, like neonatology. Micromotor-based biosensing opens a new path for future screening diagnostics; drawing new hopes in the diagnostics landscape.

Associated content

Supporting Information

Video V.3.S1. rGO/Ni/PtNPs micromotors swimming in different biological samples.

Authors information

Corresponding authors

Alberto Escarpa − Department of Analytical Chemistry, Physical Chemistry and Chemical Engineering, University of Alcalá, 28871 Alcalá de Henares, Madrid, Spain; Chemical Research Institute "Andres M. Del Rio", Universidad de Alcalá, 28871 Alcalá de Henares, Madrid, Spain; orcid.org/0000-0002-7302-0948; Email: alberto.escarpa@uah.es

Authors

Águeda Molinero-Fernández − Department of Analytical Chemistry, Physical Chemistry and Chemical Engineering, University of Alcalá, 28871 Alcaláde Henares, Madrid, Spain.

Miguel Ángel López − Department of Analytical Chemistry, Physical Chemistry and Chemical Engineering, University of Alcalá, 28871 Alcaláde Henares, Madrid, Spain; Chemical; Research Institute "Andres M. Del Rio", Universidad de Alcalá, 28871 Alcalá de Henares, Madrid, Spain.

5. References

(1)   Zha, F.; Wang, T.; Luo, M.; Guan, J. *Micromachines*. 2018, *9* (2), 78.

(2)   Khezri, B.; Mousavi, S. M. B.; Sofer, Z.; Pumera, M. *Nanoscale* 2019, *11* (18), 8825−8834.

(3)   Khezri, B.; Beladi Mousavi, S. M.; Krejcǒva ̗L.; Heger, Z.; Sofer, Z.; Pumera, M. *Adv. Funct. Mater.* 2019, *29* (4), 1806696.

(4)   Pacheco, M.; Lopéz, M. Á.; Jurado-Sańchez, B.; Escarpa, A. *Anal. Bioanal. Chem.* 2019, *411*, 1−13.

(5)   Wang, J. *Biosens. Bioelectron*. 2016, *76*, 234−242.

(6)   Kong, L.; Guan, J.; Pumera, M. *Curr. Opin. Electroche*. 2018, *10*, 174−182.

(7)   Orozco, J.; Jurado-Sańchez, B.; Wagner, G.; Gao, W.; Vazquez- Duhalt, R.; Sattayasamitsathit, S.; Galarnyk, M.; Corteś, A.; Saintillan, D.; Wang, J. *Langmuir* 2014, *30* (18), 5082−5087.

(8)   Otzen, D. *Biochim. Biophys. Acta, Proteins Proteomics* 2011, *1814* (5), 562−591.

(9)   Morales-Narvaéz, E.; Guix, M.; Medina-Sańchez, M.; Mayorga- Martinez, C.; Merkocj̗, A. *Small* 2014, *10* (13), 2542−2548.

(10)   Kagan, D.; Campuzano, S.; Balasubramanian, S.; Kuralay, F.; Flechsig, G. U.; Wang, J. *Nano Lett.* 2011, *11* (5), 2083−2087.

(11)   Balasubramanian, S.; et al. *Angew. Chem.*, Int. Ed. 2011, *50* (18), 4161−4164.

(12) Yu, X.; Li, Y.; Wu, J.; Ju, H. *Anal. Chem.* 2014, *86* (9), 4501−4507.

(13)   Vilela, D.; Orozco, J.; Cheng, G.; Sattayasamitsathit, S.; Galarnyk, M.; Kan, C.; Wang, J.; Escarpa, A. *Lab Chip* 2014, *14* (18), 3505−3509.

(14)   Orozco, J.; Pan, G.; Sattayasamitsathit, S.; Galarnyk, M.; Wang, J. *Analyst* 2015, *140* (5), 1421−1427.

(15)   Garcia-Gradilla, V.; et al. *ACS Nano* 2013, *7* (10), 9232−9240.

(16)   Esteban-Fernańdez de Ávila, B.; Zhao, M.; Campuzano, S.; Ricci, F.; Pingarroń, J. M.; Mascini, M.; Wang, J. *Talanta* 2017, *167*, 651−657.

(17)   Karshalev, E.; Esteban-Fernańdez de Ávila, B.; Wang, J. *J. Am. Chem. Soc.* 2018, *140* (11), 3810−3820.

(18)   Simon, L.; Gauvin, F.; Amre, D. K.; Saint-Louis, P.; Lacroix, J. *Clin. Infect. Dis.* 2004, *39*, 206−217.

(19)   Vashist, S. K.; Venkatesh, A. G.; Schneider, E. M.; Beaudoin, C.; Luppa, P. B.; Luong, J. H. *Biotechnol. Adv*. 2016, *34* (3), 272−290.

(20)   Kazimierczak, B.; Baraniecka, A.; Dawgul, M.; Pijanowska, D. G.; Torbicz, W.; Goŕska, M.; Grabiec, P. *Procedia Eng*. 2011, *25*, 1221−1224.

(21) Kim, T.-H.; et al. *Lab Chip* 2013, *13* (18), 3747−3754.

(22) Zhou, F.; et al. *Clin. Chem*. 2010, *56* (11), 1701−1707.

(23)   Molinero-Fernańdez, Á.; Jodra, A.;   Moreno-Guzmań, M.; Loṕez, M. Á.; Escarpa, A. *Chem. - Eur. J.* 2018, *24* (28), 7172−7176.

(24)   Maria-Hormigos, R.; Jurado-Sanchez, B.; Vazquez, L.; Escarpa, A. *Chem. Mater.* 2016, *28* (24), 8962−8970.

Supporting Information

Supporting Videos:

Video V.3.S1. rGO/Ni/PtNPs micromotors swimming in different biological samples.